Random Walk Simulation of the MRI Apparent Diffusion Coefficient in a Geometrical Model of the Acinar Tree

José M. Pérez-Sánchez,* Ignacio Rodríguez, and Jesús Ruiz-Cabello
Instituto de Estudios Biofuncionales, Universidad Complutense de Madrid, Madrid, Spain; and CIBER de Enfermedades Respiratorias, Fundación Caubet-Cimera Recinto Hospital Joan March, Mallorca, Spain

ABSTRACT Apparent diffusion coefficient (ADC) measurement in the lung using gas magnetic resonance imaging is a promising technique with potential for reflecting changes in lung microstructure. Despite some recent impressive human applications, full interpretation of ADC measures remains an elusive goal, due to a lack of detailed knowledge about the structure dependency of ADC. In an attempt to fill this gap we have performed random walk simulations in a three-dimensional geometrical model of the lung acinus, the distal alveolated sections of the lung tree accounting for ~90% of the total lung volume. Simulations were carried out adjusting model parameters after published morphological data for the rat peripheral airway system, which predict an ADC behavior as microstructure changes with lung inflation in partial agreement with measured ADCs at different airway pressures. The approach used to relate experimental ADCs to lung microstructural changes does not make any assumption about the cause of the changes, so it could be applied to other scenarios such as chronic obstructive pulmonary disease, lung development, etc. The work presented here predicts numerically for the first time ADC values measured in the lung from independent morphological measures of lung microstructure taken at different inflation stages during the breath cycle.

INTRODUCTION

The possibility of imaging gases directly within the lung may have an immediate repercussion on pulmonary physiopathology studies. Thus, MRI using hyperpolarized spin-1/2 noble gases, such as ^{3}He and ^{129}Xe, has been developed during the last 10 years (1–3) and has potential for assessing pulmonary ventilation, gas exchange, and microstructural changes (for recent reviews, see (4–6)).

Diffusion-weighted imaging of gases has been used extensively for studying chronic obstructive pulmonary diseases such as emphysema. The apparent diffusion coefficient (ADC) quantifies the mobility of a molecule within a specific medium and is related to gas properties and the topology and geometry of the medium in which the gas is embedded. Using the same gas and experimental conditions on different subjects should permit airway diameters and alveolar sizes to be compared through ADC values, even if the imaging resolution is insufficient to delineate alveolar clusters directly (7).

It has been stated in several works (7,8) that regions where lung tissue air spaces are larger, should have higher ADC values. Following this reasoning, ADC should be expected to depend on the degree of lung inflation, since, as the lung inflates to take up more gas, alveolar sacs could be expected also to inflate (especially taking into account that it is in those structures where most of the gas resides; ~90%).

Furthermore, although the influence of experimental setup and parameters on ADC measurements has been studied (9–13), there is little understanding of how the complex combination of experimental parameters and lung tissue properties end up determining ADC values. Some of the factors which could influence ADC values include degree of lung inflation, subject posture, and gas mixing, as well as random and systematic errors related to the behavior of gradient systems and other MRI hardware, ventilating devices, data processing algorithms, etc.

In this work, we have focused on creating a geometrical model (see Table 1 for geometrical parameters) of the acinar tree that reproduces the branching nature of the acinus, together with its geometrical and statistical properties (see Table 2 for statistical parameters), as well as performing simulations by setting the model parameters after known morphological data (14,15). The simulated ADC values include the value at 70% total lung capacity as well as values at 0, 5, 10, 20, and 30 mbar of relative airway pressure (relative to the atmospheric value). The values at different pressures are compared with those obtained from real ADC measurements at 2.5, 10, 15, and 20, obtaining partial correspondence.

Other geometrical models of the acinar tree have been developed. The cylinder model, developed by Yablonskiy et al. (16), treats the lung as a series of independent closed cylinders scattered randomly in all three directions. A followup of this model (17) is based geometrically on the measurements of Haefeli-Bleuer and Weibel (18). This model finds empirical relations between longitudinal and transverse ADC and geometrical parameters of airways. A similar model was developed by Fichele et al. (19), as a followup from a previous preliminary work in two dimensions (13). In this model (named the alveolar model by the authors), alveolar ducts are seen as cylinders with spheres attached around them, the spheres representing alveoli. In this model, as in the cylinder model, alveolar ducts are isolated and scattered randomly in all directions. Boundary conditions at both ends of the cylinder in the axis direction are periodic. Another

Submitted June 24, 2008, and accepted for publication April 6, 2009.

*Correspondence: iosephus@ieb.ucm.es

Editor: Michael D. Stern.

0006-3495/09/07/0656/9 $2.00

doi: 10.1016/j.bpj.2009.04.050

TABLE 1 Geometrical parameters of the acinar tree model: external diameter (2*R*), internal diameter (2*r*), and length (*L*) per generation (*Z*)

Z	2*R* (μm)	2*r* (μm)	*L* (μm)
0	346	202 (206)	295
1	346 (288)	189 (190)	266 (354)
2	346 (388)	178 (184)	240 (240)
3	346 (366)	167 (163)	216 (176)
4	346 (350)	157 (152)	195 (175)
5	346 (325)	147 (144)	176 (155)
6	346 (342)	138 (135)	158 (135)
7	346 (330)	129 (127)	143 (164)
8	346 (380)	121	128 (153)
9	346 (360)	114 (120)	116 (115)
10	346	107	104
11	346	100	95
12	346	94	85
Sac	317 (317)	133 (133)	349 (349)

The values measured by Rodríguez et al. (14) are shown in parentheses for comparison.

model, developed by Grebenkov et al. (20), treats acini as a Kitaoka labyrinth (21). In this model, a healthy acinus is represented as a three-dimensional labyrinth with dicotomic structure and nonsymmetric branches of random lengths densely filling a cube. Alveolar ducts are therefore connected, which is a significant difference from the two previous models.

As a mechanical model of the alveolar structure and dynamics, it is worth mentioning the Kitaoka 4-D model, by Kitaoka et al. (22), which presents a detailed model of the alveolus and the alveolar duct, compatible with the mechanical, morphogenetical, bifurcative, and spatial filling properties of the acinar tissue. The number of parameters and geometrical primitives of the model render the creation of a data representation of such a model in a computer program a challenging task, if acceptable computation times are to be achieved. Nevertheless, the model is to be considered as a geometrical model for performing computer simulations in the future, especially when the functional behavior of the lung tissue is to be studied.

TABLE 2 Statistical parameters per generation (*Z*) of the acinar tree model

Z	P_{bif}	N_{ducts}	N_{sacs}
0	1.00	1	0
1	1.00	2	0
2	1.00	4	0
3	1.00	8	0
4	0.75	12	4
5	0.56	14	11
6	0.42	11	16
7	0.32	7	16
8	0.24	3	11
9	0.18	1	6
10	0.13	0	2
11	0.10	0	1
12	0.08	0	0

Bifurcation probability (P_{bif}), number of ducts (N_{ducts}), and number of sacs (N_{sacs}).

The effect of collateral ventilation on long-range diffusion has also been studied by Bartel et al. (23) and Conradi et al. (24).

Diffusion MRI

The main limitation of traditional techniques for measuring diffusion is that they cannot be used for studying diffusion in vivo. It is possible to design specific magnetic resonance imaging acquisition methods directly sensitive to particle translation at a microscopic level, and thus useful for studying processes related to molecular mobility, such as diffusion.

If particle motion is such that the distances traveled by particles during the diffusion encoding time follow a Gaussian distribution, as in free diffusion, then the signal loss caused by molecular motion can be expressed as (25)

$$M = M_0\, e^{-ADC \times b}, \tag{1}$$

where M_0 is the signal intensity acquired with identical echo and repetition times (otherwise there would be also a signal loss due to relaxation), but without the diffusion encoding gradients; M the measured signal intensity; b a diffusion-weighting factor computed as the time integral of $|\vec{k}|^2$ over the k-space trajectory generated by the diffusion encoding gradients; and ADC a diffusion coefficient, which is called the apparent diffusion coefficient.

For the bipolar sinusoidal gradients normally used in our measurements, in which there is no temporal separation between the two diffusion lobes, the b-value is given by

$$b = \frac{3\gamma^2 G^2 T_{diff}^2}{8\pi^2}, \tag{2}$$

where γ is the gyromagnetic ratio, G the maximum gradient intensity of the sinusoidal lobe, and T_{diff} the total diffusion encoding time, with both sinusoidal lobes included.

In Eq. 1, b contains the information regarding the specific way in which molecular mobility was encoded into the image (gradients, timing, etc.). ADC contains information about molecular mobility itself and can be extracted on a pixel-by-pixel basis to construct an ADC image (also called an ADC map), which provides a spatial map of molecular mobility. When diffusion is restricted, the distances traveled by particles during the diffusion encoding time, in principle, do not follow a Gaussian distribution; Eq. 1 is not valid; and ADC is only the first term of a series of terms characterizing signal attenuation (26,27). Nevertheless, if deviation from the Gaussian distribution is not so big, an ADC value can still be approximately computed using Eq. 1 and used as a measure of particle mobility. In this case, the ADC value is not only determined by molecular mobility; it also depends on the diffusion encoding time and the shape of the diffusion-encoding gradient. This dependence provides us with the possibility of choosing diffusion-encoding parameters to make ADC more or less sensitive to geometry and size changes in a desired length scale or a given shape; but on

the other hand, it adds a relative character to ADC measurements which has to be taken into account when trying to relate ADC to the geometry and size of the structure in which the diffusing medium is contained. This dependence of ADC on factors other than molecular mobility and recipient structure is the reason for the word ''apparent'' appearing in the ADC acronym.

For constructing the ADC map, it suffices to acquire several diffusion-weighted images with different values of b. Changing b for this purpose should be done by changing diffusion encoding gradient intensity, while keeping diffusion encoding time and encoding gradient shape unchanged. Echo and repetition times should be the same for all images, so that any effect of spin relaxation on image intensity is automatically left out when extracting ADC.

Once the images have been acquired and reconstructed, the intensity values of each pixel for the different images should be fitted to an exponential using the corresponding b-values.

Among other things, ADC imaging is used for characterizing organic tissue, and it has already found extensive application for studying diffusion taking place in the brain, using proton imaging, and in the lung, performing imaging of gases.

MATERIALS AND METHODS

Since signal attenuation in diffusion-weighted images is caused only by the kinematics of the random motion of particles, the random-walk kind of numerical simulations is a good candidate for predicting signal attenuation and resulting ADC values. In our simulations, the time T_{diff}, during which the whole bipolar diffusion encoding gradient is applied, is divided into N intervals of duration $\delta t = T_{\text{diff}}/N$ in which the gradient value is computed based on the gradient shape and the particle is moved a random distance in a random direction.

In this work, numerical simulations were carried out first in a cylinder with the diffusion encoding gradient perpendicular to the axis, which is a case that can be described theoretically, and hence can provide some validation of the simulation technique. The theoretical calculations of ADC for a cylinder were performed in a similar way as Yablonskiy et al. (16), this time using a sinusoidal gradient, to perform a validation of the simulation algorithm and implementation, and detect any gross error in the implementation. The results obtained for the simulation in an infinite cylinder were in very good agreement with the theoretical values.

Spatial displacements, phase and signal

In our simulations, we select the displacements in each of the coordinate directions independently using identical Gaussian probability distributions. The displacements have zero mean and standard deviation given by

$$\sqrt{2D\,\frac{T_{\text{diff}}}{N}}, \tag{3}$$

while the particle does not reach a recipient wall. Each time a new random displacement is calculated it is checked whether the corresponding trajectory would cross any of the recipient walls; if this were the case, the computed displacement is discarded and a new one is computed randomly. This means that although the probability distribution used for computing candidate displacements is Gaussian, the final displacement distribution is not Gaussian as a result of the selection rules used to simulate restriction.

The phase changes of the particles are computed for each iteration based on the gradient value and the position, and added to get the net phase accumulated during the whole time T_{diff}. The relative phase change in any given iteration over a small time increment δt is given by

$$\delta\phi = \vec{G} \cdot \vec{r}\,\delta t, \tag{4}$$

where $\vec{G}$ and $\vec{r}$ are the gradient and position values, respectively, during the iteration, which are computed once and considered constant during each iteration. The collective magnetization of the sample, as a vector, is computed adding the individual magnetization vectors of all spins. Since the spin magnetization magnitude is constant, changes in the net magnetization of the sample are determined solely by the changes in the phase distribution of spins due to the diffusion-encoding gradient.

The acinar tree model

Notwithstanding the usefulness of numerical simulation of diffusion in simple structures to understand some basic properties of ADC, it is quite improbable that we can understand diffusion and the properties of ADC in a complex structure, such as the lung, from them. The lung is a complex porous medium with numerous interconnected structures, thus, the need for models that reflect lung structure faithfully within the limits of our present computing capacity. In this work, we show the results of simulating diffusion and ADC measurements in a three-dimensional geometrical model of the acinus.

Lung structure

Lung topology is that of irregular dichotomy. Starting from a first branch, the trachea, successive bifurcations take place; the first splits the trachea into two bronchi, one for each lung, and the structure keeps bifurcating a number of times, or generations, the number of which depends on the species.

The first generations of the lung tree exclusively deliver gas to the more distal generations. Starting from a certain generational number (or a range of them), alveoli start appearing in the walls of the tubular airways. Finally, the last generations are densely populated with alveoli, increasing the volume corresponding to the alveoli and decreasing the volume corresponding to the central transport section as the generation number increases.

The first branches with alveoli as we move down the tree are called terminal bronchioles and each portion of the tree distal to one of them is called an acinus. Each alveolated branch between two nodes of one acinus is called an alveolar duct and the very terminal structures, most densely populated with alveoli, where bifurcation stops, are called the alveolar sacs.

Bicylindrical coaxial alveolar duct model

It is well known that most of lung volume—~90%—corresponds to the acinar part of the tree (14), so it is reasonable to expect that acinar properties play a key role in determining the ADC values measured in the lung. This is especially true for short-range diffusion, in which gas particles mainly stay within the same structures during ADC measurement.

The probably most extended idea of an alveolar duct is that of a more or less cylindrical construct with many smaller spheres attached to the wall, and something similar happens with the alveolar sacs, imagined as something similar to a bunch of grapes. This idea of a well-defined central structure with independent spheres attached, even being popular enough to make its way into some medicine text books, is not very accurate; it is not to say that alveoli are not distributed around some central structure, but rather than being independent structures, they are attached to each other in a compact manner, sharing their walls so that they are not spheres, but some kind of convex polyhedra with curved walls. It should be pointed out that size and shape of the structures forming the acinus change during the respiratory cycle.

An alveolar duct model (28) studied by Paiva (29) and Verbanck and Paiva (30) is that of two coaxial cylinders with the space between them divided by radial and transversal walls spaced at constant angles and lengths. The result is a number of alveolar compartments in the outer shell surrounding a central cylindrical transport section, in which the wall of each compartment in the

inner cylinder has an opening for ventilation. Paiva and Verbanck solved, numerically, the gas transport equations in this model (29,30), reduced to a two-dimensional representation thanks to its axial symmetry. They obtained a diffusion coefficient given by the free diffusion coefficient times the ratio between the inner and outer transversal sections of the structure. A three-dimensional representation of the alveolar duct model can be found in Fig. 1. A detailed study of nuclear magnetic resonance diffusion experiments in a three-dimensional version of this alveolar duct model have been carried out very recently by Sukstanskii and Yablonskiy (17).

This alveolar duct model requires several independent parameters to be fully characterized: inner and outer radii, length, number of sections in the axial and angular direction, and at least one parameter determining alveolar mouth size.

Whole acinar tree model

We now propose a model of the whole acinus: a tree characterized by a series of parameters mapping topology, geometry, and statistical properties to generational number, so that changing these parameters we could reproduce the properties of the acinus in different species. The bicylindrical coaxial model discussed in the previous section is the basic element for building this acinar tree model, in which the acinar tree is modeled as a collection of bicylindrical coaxial ducts with different parameters assigned to them and connected at the tree nodes.

Our model bifurcates from an initial terminal bronchiole with each duct between two nodes having an inner radius (central section), an outer radius (central section plus alveoli), and a length. These parameters are computed for each generation multiplying the values of the previous generation by three constant factors, one for each of the parameters.

Bifurcation probability can be constant during a number of initial generations and then decrease geometrically, being multiplied by a factor <1 from each generation to the next, until bifurcation stops spontaneously. Each node, at the end of one generation and the beginning of the next, can have ducts connected if the tree bifurcates further in a given direction, or sacs if bifurcation stops for a given branch; so there are three kinds of possible nodes at the end of any given duct, those with two ducts connected, those with a duct and a sac, and those terminal nodes having two sacs attached. Since bifurcation in a given node of the tree does not happen always in the same way, but is determined by some probability, there could be different acini with the same parameters and statistical properties but different particular branches.

Regarding the branching spatial properties of the acinar tree, at each bifurcation the angle between two children is 80°, constant for the whole acinus, and the bifurcation plane is rotated 90° at each node around the axis of the parent with respect to the plane formed by the parent and its sibling.

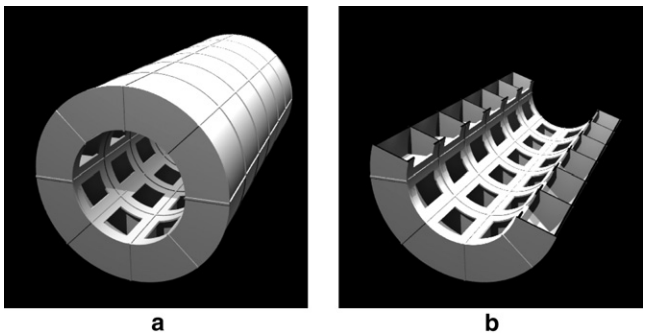

FIGURE 1 Three-dimensional representation of the bicylindrical coaxial alveolar duct model. This model requires several independent parameters to be fully characterized: inner and outer radii, length, number of sections in the axial and angular direction, and at least one parameter determining alveolar mouth size. (*a*) Whole duct. (*b*) Axial cut allowing us to see the interior of the structure.

To perform numerical simulations on more than one acinus, each computing thread of the simulation program generates its own acinus using the same parameters at the beginning of the simulation.

Each duct in the acinar tree model corresponds to the bicylindrical coaxial model shown before. A three-dimensional representation of the whole acinar tree can be seen in Fig. 2.

Diffusion gradient orientation is chosen randomly for each particle, simulating the fact that acini are oriented in all spatial directions in the lung. The initial positions of the particles are assigned randomly, taking into account the volume of each duct. The probability for a given particle to have initial position in a given duct equals the ratio of the duct volume to the total acinar volume.

Particle movement inside the ducts is restricted by the walls represented with solid lines in Fig. 3; when the particle goes out through the central section of one of the ends of the cylinder, movement starts to be simulated in another cylinder, chosen by the following rules:

- If the new position of the particle is in a region inside a single cylinder (*lighter shading* in the figure), that cylinder is chosen.
- If the new position is in a region shared by two cylinders (*darker shading*), one of them is chosen with probability 1:2 for each candidate.
- If the new position is in a region in which no cylinders exist, or if a particle reaches the beginning of the acinar tree, the displacement is discarded.

Two of the parameters characterizing the alveolar duct model (the number of angular and the number of transversal sections) control the number of alveoli per duct, and changing them allows us to simulate the hypothesis known as alveolar recruitment (31,32).

The size of the alveolar compartments in our model is characterized by three parameters: Depth in the radial direction, which is the difference between the outer and the inner radius,

$$d = R - r, \tag{5}$$

a length in the Z direction, determined by duct length and the number of transversal sections n_Z,

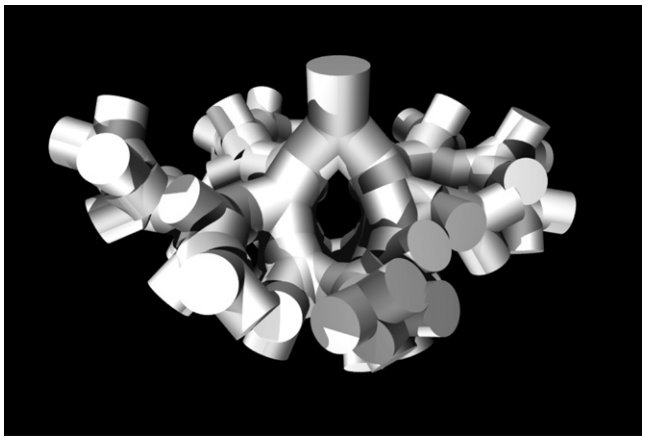

FIGURE 2 Three-dimensional representation of the acinar tree model. Each duct between two nodes corresponds to the bicylindrical coaxial alveolar duct model with inner radius, an outer radius, and length computed for each generation multiplying the values of the previous generation by three constant factors, one for each of the parameters. Bifurcation probability can be constant during a number of initial generations and then decrease geometrically until bifurcation stops spontaneously. The angle between siblings is 80° and the bifurcation plane at each node is rotated 90° with respect to the previous bifurcation plane, where the parent node and its sibling are located.

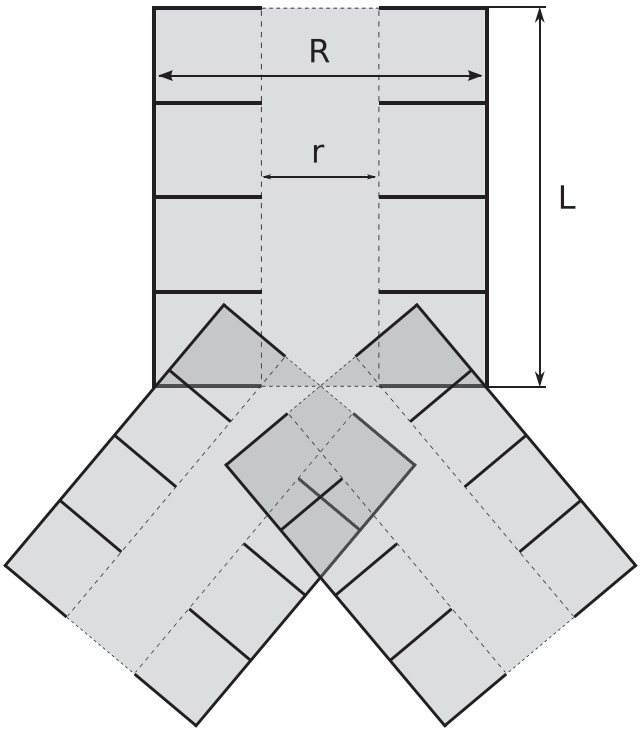

FIGURE 3 Scheme of a bifurcation in the acinar tree. Alveolar mouths have not been represented, in order to keep the drawing as clear as possible.

$$l = \frac{L}{n_Z}, \tag{6}$$

and a length in the angular direction, determined by both radii and the number of angular sections n_θ. The length of the arc with radius $(R + r)/2$ and angle corresponding to the alveolar compartment has been taken, which is

$$a = \frac{\pi(R + r)}{n_\theta}. \tag{7}$$

The volume of each alveolar compartment is given by

$$v = \frac{\pi\left(R^2 - r^2\right)L}{n_\theta\, n_Z}. \tag{8}$$

Implementation

The software for numerical simulations was developed in-house using the "C" programming language. It uses the Mersenne Twister random number generator converting the uniformly distributed integer random numbers resulting from this algorithm into double-precision, floating-point numbers following a Gaussian distribution.

Simulations were run in a dual processor computer with Xeon processors clocking at 2.4 GHz and 2 GB of total RAM. The simulation code was compiled using the 4.1.2 version of GCC, the GNU C Compiler, and run in parallel in the two processors using 16 threads managed by a 2.6.17 SMP capable Linux kernel. Each run moved 10^5 particles whose initial positions were randomly and homogeneously distributed inside the recipient and the diffusion encoding time was divided into 10^5 intervals. A complete ADC experiment takes 2–3 h to simulate.

RESULTS AND DISCUSSION

Reproduction of the real acinus

Since the model has been used for simulating ^{3}He diffusion in the rat lung, the first step has been to fit the model parameters to reproduce the properties of the rat acinus as measured by Rodríguez et al. (14). The values of the model parameters for this case are the following: Bifurcation probability has been fixed to one for the first four generations and then decreased by a geometric factor of 0.75. For the external duct diameter $2R$, the constant value 346 μm has been used, and for the inner diameter $2r$ the initial value of the radius was 202 μm and the decrease factor was 0.94. Duct length L was set to an initial value of 295 μm and decreased by a factor of 0.9 from each generation to the next. Table 3 shows the values of the global geometrical and statistical parameters.

ADC at 70% total lung volume

In an acinar tree with the parameters published by Rodriguez et al. (14) for the rat lung inflated at 70% total lung capacity, simulating the ^{3}He ADC measurement with a bipolar sinusoidal gradient of duration 1.5 ms and four b-values yields ADC values of 0.1024 cm^2/s and 0.1147 cm^2/s, for free diffusion coefficients of 1.4 cm^2/s and 1.91 cm^2/s, respectively. The two values of the free diffusion coefficient correspond to helium with ~25% air (1.4 cm^2/s) and pure helium (1.91 cm^2/s) at 20°C (33); all the simulations have been performed for both values of the free diffusion coefficient to estimate the possible influence of residual air in the lungs during measures. Fig. 4 shows the exponential fit of the simulated data performed. A mouth aperture value of 0.7 was used.

ADC dependence on lung inflation

The model of the acinar tree has been also fitted to the morphometrical data published by Mercer et al. (15) to simulate

TABLE 3 Global statistical and geometrical parameters of the acinar tree model

Parameter	Model (n = 1000)	Measured (n = 7)
N_{ducts}	65	63
N_{sacs}	64	64
$\overline{Z}_{\text{sacs}}$	6.7	6.1
Z_{sacs} range	4–10	4–8
Z_{sacs} mode	6.44	6
Branching factor X_Z	1.87	1.93
Volume (mm^3)	2.16	2.17*
Mean path $\overline{L}_p$ (mm)	1.63	1.46

The second column shows the mean values of our model computed over 1000 acini and the third shows the mean values over seven acini measured by Rodríguez et al. (14). $\overline{Z}_{\text{sacs}}$ is the mean generation number of sacs in one acinus averaged over the different acini; the range is given by the average over different acini of the first and last generation where sacs are present and the mode is the value of the generation number Z where the number of sacs is maximum. The branching factor is computed as $X_{\overline{Z}} = (N_{\text{sacs}})^{1/\overline{Z}_{\text{sacs}}}$. $\overline{L}_p$ is the mean path along the tree from the entrance of the acinus to a sac.
*Total acinar volume divided by the number of acini in the lung.

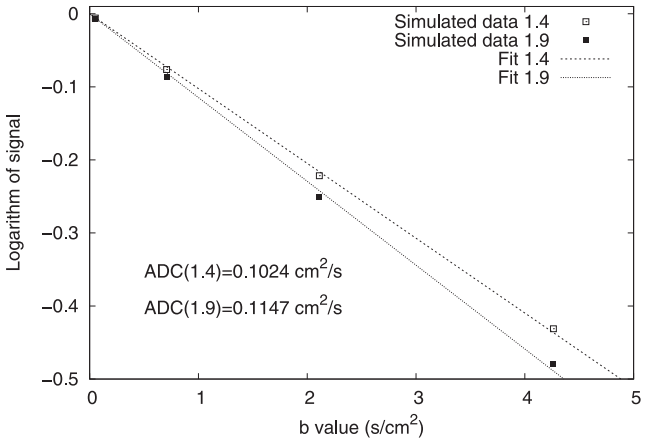

FIGURE 4 Exponential fit of the signal attenuation values for the simulation of the pure ^{3}He ADC measurement with free diffusion coefficients 1.4 and 1.91 cm^2/s, and a bipolar sinusoidal gradient of duration 1.5 ms in the acinar tree model adjusted to reproduce 70% total lung capacity.

the behavior of ADC as the lung inflates from functional residual capacity to total lung capacity.

In the work by Mercer et al., alveolar dimensions and the portion of gas in the inner section of the alveolar ducts are reported from null relative pressure to 30 mbar. In principle, using Eqs. 5–8 it should be possible to compute the inner and outer radii of our model at different pressures. However, due to the difference in shape of complex real alveoli and any simple geometrical structure, matching model dimensional parameters directly to measured alveolar sizes leads to differences in volume and hence in the space available for diffusion. This difference can be corrected introducing the shape coefficient,

$$\beta = \sqrt{\frac{\overline{D^3}}{\overline{V}}}, \tag{9}$$

where $\overline{D}$ and $\overline{V}$ are mean alveolar size and volume, respectively (34). To compute the inner and outer radii of our model, we adjusted the value of β to $\beta = 1.85$, as reported by Randell et al. (34) for control rats 21 days old. This is performed by dividing the volume in Eq. 8 by β^2 after considering $a = l = d$. Cylinder lengths and geometrical factors from one generation to the next have been set to the values deduced from Rodriguez et al. (14) for all pressure values. The values obtained for the radii are shown in Table 4. The n_θ and n_Z parameters have been adjusted so that alveoli have values as similar as possible for the three parameters characterizing alveolar dimensions; this makes the number of alveoli different at each pressure, which resembles a behavior similar to that found in alveolar recruitment.

Fig. 5 shows the results of the simulations compared with the ADC values measured in the rat lung at some of the pressures (9). These experimental values correspond to in vivo ADC measurements performed using the same experimental conditions as the ones used in the computer simulation (a bipolar sinusoidal gradient with duration 1.5 ms and the four b-values shown in Fig. 4). The rat lungs were washed twice with pure ^{3}He to remove residual air in the lungs prior to the ADC acquisition. It can be appreciated from Fig. 5 and Table 4 that the ADC values resulting from the simulation in the model are very tolerant to residual presence of air. A very good correspondence can be observed at some values (10 mbar), whereas at 5 and 20 mbar there is some discrepancy between the simulated and measured values; for the extreme values (0 and 30 mbar) ADC measurements were not available. Sources of discrepancy may be due to model inaccuracy, morphological data inaccuracy and the fact that the ^{3}He concentration and temperature (and therefore the free diffusion coefficient) inside the rat lungs was not precisely known, even if this last effect is too small to account for the discrepancy on its own.

Comparison with other models

Other numerical models have been used and reported in the literature. The acinar model developed in this article will be compared to four of them: the cylinder model, by Yablonskiy et al. (16), the alveolar model, by Fichele et al. (19), the labyrinth model, by Grebenkov et al. (20), and the cylinder-plus-alveolar-sleeve duct model, by Sukstanskii et al. (17).

The cylinder model is a theoretical model, in which the expected signal attenuation is calculated, taking into account cylinder size and gradient orientation and assuming the Gaussian phase distribution approach to be valid. This model was the first to address the relationship between diffusion measurements and lung microstructure. The Gaussian phase distribution approach is known not to be valid, the effect of

TABLE 4 Values for the model parameters deduced from the measurements of Mercer et al. (15) at different relative pressures (*P* given in mbar), with and without volume correction

P	r_0 (μm)	R_0 (μm)	α	ADC_{min}	ADC_{max}
0	25 (52)	64 (83)	0.43	0.0323 (0.0713)	0.0437 (0.0876)
5	74 (141)	108 (156)	0.63	0.0884 (0.1373)	0.1053 (0.1535)
10	128 (237)	178 (256)	0.78	0.1289 (0.2174)	0.1481 (0.2398)
20	98 (192)	150 (217)	0.73	0.0979 (0.1714)	0.1162 (0.1874)
30	157 (277)	203 (289)	0.74	0.1475 (0.2549)	0.1645 (0.2754)

The values without volume correction are given in parentheses. Minimum and maximum ADC values are those resulting from simulating with the free diffusion coefficients 1.4 and 1.91 cm^2/s, corresponding to a mixture of ^{3}He with ~25% air and pure ^{3}He, respectively. The mouth-opening parameter α does not change with volume correction.

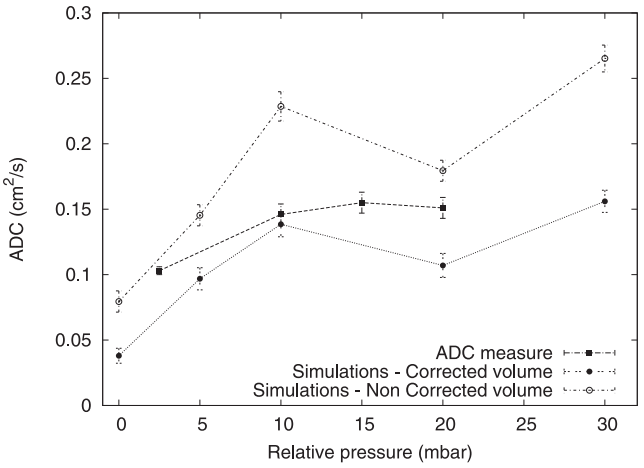

FIGURE 5 Simulation results at different pressures compared to ADC measurements in the rat lung. The points corresponding to the simulations are shown with a bar covering the ADC values obtained from several simulations in the 1.4–1.9 cm^2/s range of the free diffusion coefficient. The extremes of this range correspond to 25%Air + ^{3}He (1.4) and pure helium (1.91). The random error of the ADC simulation is described in Convergence of the Simulations. ADC measurements are reported as the average of measures carried out on six different animals, with the standard deviations represented with error bars.

this lack of Gaussian distribution being more important as the diffusion gradient strength increases (26,27). As a result, morphological sizes can be biased if estimated from ADC measurements. Another shortcoming of this model is the lack of connectivity among cylinders, which represent alveolar ducts. These shortcomings have been addressed in a followup work (17). In this followup work, relationships between longitudinal and transverse diffusion coefficients and the geometrical parameters of airways and alveoli are found by Monte Carlo simulations. In addition, the effects of non-Gaussian signal behavior are taken into account.

The alveolar model is a finite difference model, in which the Bloch-Torrey equations are numerically solved. Improvements over the previous model are that it does not rely on the phase distribution being Gaussian, and also that the geometry is more elaborate. Shortcomings of this model are that in the model all alveolar ducts are equal in size and they are not connected among them. However, these two effects have been studied by the same authors in a two-dimensional model (13), and the same techniques could be used to extend the alveolar model.

The labyrinth model is a random walk model, in which alveolar ducts are represented by cubes connected in a Kitaoka labyrinth way. An improvement over the previous models is that alveolar ducts are simply connected, using dichotomous branching, as is the case in real acini. Shortcomings of this model are that all alveolar ducts have the same size, and also that when a duct bifurcates, one of its children is parallel to the father and the other one is perpendicular to it.

The model described in this article addresses all shortcomings enumerated below, even if it has shortcomings of its own. In our model, the possibility of simulating tissue destruction and collateral communication among alveolar ducts within an acinus, as may happen in emphysema, has not been implemented yet. This is possible and straightforward to implement using the labyrinth model. Also, ensuring complete spatial filling has not been taken into account by the branching algorithm. Improving the model to address these lacks and incorporating other features should be a topic in our future research.

Convergence of the simulations

The numerical simulations carried out here result from a numerical integration of the effect of the diffusion gradient over the phase distribution of the spins. On the one hand, the effect of the gradient is integrated over time, using as integration interval the diffusion-encoding time T_d; on the other hand, the effect of the gradient is averaged over a great number of trajectories sampling the space inside the container. Regarding these two procedures, the diffusion-encoding time T_d divided by the number of integration steps is the time differential for numerical integration and the number of spins or trajectories used determine the sampling of space inside the container.

The greater the number of steps and the number of spins, the better our simulation, but an infinite number for any of those values is not possible. That is why before simulating it is a must to determine which values of these parameters yield values are accurate enough for our purposes, while keeping simulation time within reasonable values.

Convergence error caused by too small a number of steps or spins is of a different nature. A small value in the number of steps causes a systematic integration error that decreases as the number of steps increases. The error related to the number of spins is of a random nature, corresponding to an insufficient sampling of a probability distribution, and its typical value decreases as the number of spins increases.

The random error was measured as the relative standard deviation taken over 10 identical simulations and the systematic error as the relative change when the number of steps is increased one order-of-magnitude beyond the chosen value.

We characterized these errors before the simulation and fixed the values to 10^5 for the number of spins and 10^5 for the number of steps. The exact degree of convergence is different for each simulation, since it depends on the values chosen for the model parameters and the free diffusion coefficient, but the random and systematic errors of all results shown here are $<4\%$ and are typically ~2% or lower.

CONCLUSIONS

The results presented here can lead to two completely different interpretations about whether ADC is a good tool for diagnosing lung disease: On the one hand, it could be stated that ADC is not a good predictor, since it cannot be

expected to behave always in the same manner; but on the other hand, different behaviors under different kinds of tissue damage and experimental conditions could make it a fine-tuned indicator.

Making a decision about ADC usefulness will still take more experimentation and modeling. Although some studies successfully relate ADC values to the value of histopathological measures (8,36), many aspects of ADC behavior in complex media are poorly understood and knowledge about ADC relation to in vivo physiological lung parameters is rather scant. Furthermore, ADC results have to be interpreted always in the light of experimental parameters (i.e., mixture composition and pressure) and the different ways in which healthy and diseased lungs respond and interact with them.

A geometrical model of the lung acinus has been developed in this article. This model addresses shortcomings of earlier acinar models, even if it has shortcomings of its own. The main shortcomings of this model are that it does not reproduce the polyhedral shape of the alveoli and the spatial filling properties of the lung tissue. Combining this model with Monte Carlo numerical simulations, a partial correspondence can be seen between simulated and real ADC measurements in healthy rat lungs. This acinar tree model can, in principle, be used to simulate other processes taking place in the lung, such as other aspects of diffusion, convection, blood-airway gas exchange, just to name a few. Furthermore, for these and other feasible studies, gas behavior could be described combining the geometrical acinar tree model shown here with other simulation methods apart from Monte Carlo.

We thank Prof. Manuel Paiva and Dr. Sylvia Verbanck for their enlightening discussions.

This research was supported by grants from the Spanish Comisión Interministerial de Ciencia y Tecnología (CICYT No. NAN2004-08805 and No. SAF2008-05412), from the European union (No. MRTN-CT-2006-036002), and from the Autonomous Community of Madrid (No. S0505-AGR-187).

REFERENCES

1. Albert, M. S., G. D. Cates, B. Driehuys, W. Happer, C. S. Springer, Jr., et al. 1994. Biological magnetic resonance imaging using laser polarized ^{129}Xe. *Nature.* 370:199–201.
2. Saam, B. T., D. A. Yablonskiy, V. D. Kodibagkar, J. C. Leawoods, D. S. Gierada, et al. 2000. MR imaging of diffusion of ^{3}He gas in healthy and diseased lungs. *Magn. Reson. Med.* 44:174–179.
3. Mayo, J. R., and M. E. Hayden. 2002. Hyperpolarized helium-3 diffusion imaging of the lung. *Radiology.* 222:8–11.
4. Möller, H. E., X. J. Chen, B. Saam, K. D. Hagspiel, G. A. Johnson, et al. 2002. MRI of the lungs using hyperpolarized noble gases. *Magn. Reson. Med.* 47:1029–1051.
5. Kauczor, H. U. 2003. Hyperpolarized helium-3 gas magnetic resonance imaging of the lung. *Top. Magn. Reson. Imaging.* 14:223–230.
6. Van Beek, E. J. R., J. M. Wild, H. U. Kauczor, W. Schreiber, J. P. Mugler, et al. 2004. Functional MRI of the lung using hyperpolarized 3-helium gas. *J. Magn. Reson. Imaging.* 20:540–554.
7. Chen, X. J., L. W. Hedlund, H. E. Möller, M. S. Chawla, R. R. Maronpot, et al. 2000. Detection of emphysema in rat lungs by using magnetic resonance measurements of ^{3}He diffusion. *Proc. Natl. Acad. Sci. USA.* 97:11478–11481.
8. Peces-Barba, G., J. Ruiz-Cabello, Y. Cremillieux, I. Rodríguez, D. Dupuich, et al. 2003. ^{3}He MRI diffusion coefficient correlation to morphometry in a model of mild emphysema. *Eur. Respir. J.* 22:14–19.
9. Pérez-Sánchez, J. M., D. Rudersdorf, T. Kaulisch, I. Rodríguez, G. Peces-Barba, et al. 2006. Pressure dependence, isotropy, and reproducibility of in-vivo ^{3}He-MRI ADC measurements in the rat lung at 0.5T. *In* Proceedings of the 3rd International Workshop of Pulmonary Functional Imaging. 66. http://www.iwpfi.dkfz.org/images/proceedings_iwpfi2006.pdf.
10. Acosta, R. H., P. Blümler, L. Agulles-Pedrós, A. E. Morbach, J. Schmiedeskamp, et al. 2006. Controlling diffusion of ^{3}He by buffer gases: a structural contrast agent in lung MRI. *J. Magn. Reson. Imaging.* 24:1291–1297.
11. Ruiz-Cabello, J., J. M. Pérez-Sánchez, R. Pérez de Alejo, I. Rodriguez, N. González-Mangado, et al. 2005. Diffusion-weighted ^{19}F-MRI of lung periphery: influence of pressure and air-SF6 composition on apparent diffusion coefficients. *Respir. Physiolo. Neurobiol.* 148:43–56.
12. Schreiber, W., A. Morbach, T. Stavngaard, K. Gast, A. Herweling, et al. 2005. Assessment of lung microstructure with magnetic resonance imaging of hyperpolarized helium-3. *Respir. Physiolo. Neurobiol.* 148:23–42.
13. Fichele, S., M. N. J. Paley, N. Woodhouse, P. D. Griffiths, E. J. R. van Beek, et al. 2004. Investigating ^{3}He diffusion NMR in the lungs using finite difference simulations and in vivo PGSE experiments. *J. Magn. Reson.* 167:1–11. http://dx.doi.org/10.1016/j.jmr.2003.10.019.
14. Rodríguez, M., S. Bur, A. Favre, and E. R. Weibel. 1987. Pulmonary acinus: geometry and morphometry of the peripheral airway system in rat and rabbit. *Am. J. Anat.* 180:143–155.
15. Mercer, R. R., J. M. Laco, and J. D. Crapo. 1987. Three-dimensional reconstruction of alveoli in the rat lung for pressure-volume relationships. *J. Appl. Physiol.* 62:1480–1487.
16. Yablonskiy, D. A., A. L. Sukstankii, J. C. Leawoods, D. S. Gierada, G. L. Bretthorst, et al. 2002. Quantitative in vivo assessment of lung microstructure at the alveolar level with hyperpolarized ^{3}He diffusion MRI. *Proc. Natl. Acad. Sci. USA.* 99:3111–3116.
17. Sukstanskii, A. L., and D. A. Yablonskiy. 2008. In vivo lung morphometry with hyperpolarized ^{3}He diffusion MRI: theoretical background. *J. Magn. Reson.* 190:200–210.
18. Haefeli-Bleuer, B., and E. R. Weibel. 1988. Morphometry of the human pulmonary acinus. *Anat. Rec.* 220:401–414.
19. Fichele, S., M. N. J. Paley, N. Woodhouse, P. D. Griffiths, E. J. R. V. Beek, et al. 2004. Finite-difference simulations of ^{3}He diffusion in 3D alveolar ducts: comparison with the ''cylinder model. *Magn. Reson. Med.* 52:917–920.
20. Grebenkov, D. S., G. Guillot, and B. Sapoval. 2007. Restricted diffusion in a model acinar labyrinth by NMR: theoretical and numerical results. *J. Magn. Reson.* 184:143–156.
21. Kitaoka, H., S. Tamura, and R. Takaki. 2000. A three-dimensional model of the human pulmonary acinus. *J. Appl. Physiol.* 88:2260–2268.
22. Kitaoka, H., G. F. Nieman, Y. Fujino, D. Carney, J. Dirocco, et al. 2007. A four-dimensional model of the alveolar structure. *J. Physiol. Sci.* 57:175–185.
23. Bartel, S.-E. T., S. E. Haywood, J. C. Woods, J. V. Chang, C. Menard, et al. 2008. Role of collateral paths in long-range diffusion in lungs. *J. Appl. Physiol.* 104:1495–1503.
24. Conradi, M. S., D. A. Yablonskiy, J. C. Woods, D. S. Gierada, S.-E. T. Bartel, et al. 2008. The role of collateral paths in long-range diffusion of ^{3}He in lungs. *Acad. Radiol.* 15:675–682.
25. Stejskal, E., and J. Tanner. 1965. Spin diffusion measurements: spin echoes in the presence of a time-dependent field gradient. *J. Chem. Phys.* 42:288–292.
26. Jacob, R. E., G. Laicher, and K. R. Minard. 2007. 3D MRI of non-Gaussian ^{3}He gas diffusion in the rat lung. *J. Magn. Reson.* 188:357–366.
27. Grebenkov, D. S. 2007. NMR survey of reflected Brownian motion. *Rev. Mod. Phys.* 79:1077–1137.

28. Weibel, E. R. 1963. Morphometry of the Human Lung. Springer-Verlag, New York.

29. Paiva, M. 1974. Gaseous diffusion in an alveolar duct simulated by a digital computer. *Comput. Biomed. Res.* 7:533–543.

30. Verbanck, S., and M. Paiva. 1998. Effective axial diffusion in an expansive alveolar duct model. *Respir. Physiol.* 73:273–278.

31. Smaldone, G. C., W. Mitzner, and H. Itoh. 1983. Role of alveolar recruitment in lung inflation: influence on pressure-volume hysteresis. *J. Appl. Physiol.* 55:1321–1332.

32. Escolar, J. D., and A. Escolar. 2004. Lung hysteresis: a morphological view. *Histol. Histopathol.* 19:159–166.

33. Bidinosti, C. P., J. Choukeife, P.-J. Nascher, and G. Tastevin. 2003. In vivo NMR of hyperpolarized ^{3}He in the human lung at very low magnetic fields. *J. Magn. Reson.* 162:122–132.

34. Randell, S. H., R. R. Mercer, and S. L. Young. 1989. Postnatal growth of pulmonary acini and alveoli in normal and oxygen-exposed rats studied by serial section reconstruction. *Am. J. Anat.* 186: 55–68.

35. Reference deleted in proof.

36. Woods, J. C., C. K. Choong, D. A. Yablonskiy, J. Bentley, J. Wong, et al. 2006. Hyperpolarized ^{3}He diffusion MRI and histology in pulmonary emphysema. *Magn. Reson. Med.* 56:1293–1300.